MLF Experimental Report	提出日 Date of report 25/Jul/2013
実験課題番号 Project No. 2012P0601 実験課題名 Title of experiment Development of fundamental techniques for pulsed neutron imaging 実験責任者名 Name of principal investigator Yoshiaki Kiyanagi 所属 Affiliation Hokkaido University	装置責任者 Name of responsible person Kenichi Oikawa 装置名 Name of Instrument/（BL No.） BL10 利用期間 Dates of experiments 13/May/2012 – 16/May/2012 1/Jun/2012 – 3/Jun/2012 11/Jun/2012 25/Jun/2012 – 28/Jun/2012 5/Dec./2012 – 6/Dec./2012 14/Dec./2012 – 17/Dec./2012 17/Jan./2013 – 19/Jan./2013 17/Mar./2013 – 19/Mar./2013

1．研究成果概要（試料の名称、組成、物理的・化学的性状を明記するとともに、実験方法、利用の結果得られた主なデータ、考察、結論、図表等を記述してください。

Outline of experimental results (experimental method and results should be reported including sample information such as composition, physical and/or chemical characteristics.

Ⅰ.Bragg edge imaging

I.1 Transmission experiment on high temperature alloys

(1) Sample: Inconel

(2) Experimental procedure and results

High temperature alloys (HTA) need superior ability of creep strength, resistivity for thermal cycle fatigue and hot gas corrosion. So far, optimization of the properties has been achieved by the improvement of the properties of initial component adjustment. But the desired properties are sometimes disappeared by the effect, such as age precipitation or subsequent welding. Therefore, we apply the neutron transmission spectroscopy technique to the microstructure investigation of HTA which has the controlled grain boundary for the improvement of engineering properties. The aim of the study is the analysis of the change in crystal microstructure by the friction stir welding (FSW) of Inconel 600 alloy.

The measurements were performed with the 256ch Li glass detector set on the 14 m position at BL10. The alloy samples were installed to its front. The source power of the MLF was around 220 kW. We chose the rotary collimator size small and the beam was narrowed down to 50 mm × 50 mm by the B_4C slit at the beam tube exit. Fig. 1 shows the imaging results of FSW samples. These are obtained by visualizing the value obtained by the integration of the transmission between the first and the second Bragg-edge wavelength. They are adjusted for friction stir position to come to the right at 25 mm position on the vertical axis. The order of the samples, FSM4, FSM6 and FSM8, are corresponded from lowest rotational speed of the friction stir. From the figure we can recognize the transmission intensity is lower particularly for FSM4 and FSM8 compared with FSM6. There is a

possibility that certain change in micro structure, such as the change of the crystallite size, is generated in them. However, comparing the shapes of the transmission spectra of these samples, significant changes have not been observed. This means that the strong texture is not formed in the process.

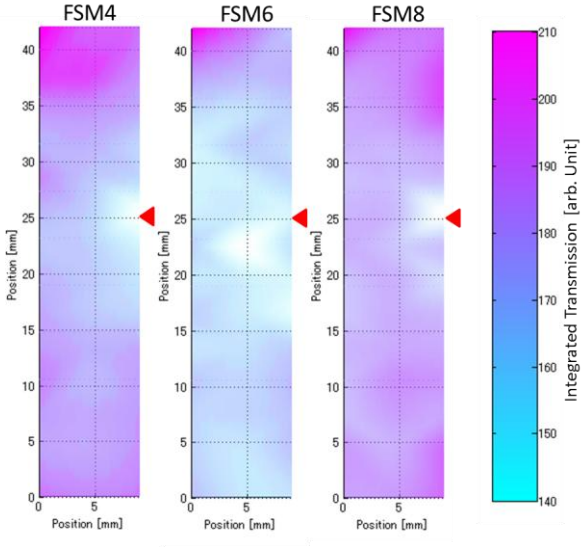

Fig. 1 Transmission images for the friction stir welding (FSW) samples of Inconel 600 alloy. The red triangles indicate the welding point, respectively.

I.2 Demonstration experiment on axisymmetric strain tomography by Bragg-edge neutron transmission spectroscopy with the tensor CT method

(1) Sample: VAMAS cylinder (neutron strain-stress analysis international standard material, Aluminum, Bulk, 5 cm diameter×5 cm height)

(2) Experimental procedure and results

In this experiment, we tried to quantitatively reconstruct two-dimensional cross-sectional image of axisymmetric strain distribution in the VAMAS cylinder (neutron strain-stress analysis international standard material, Aluminum, Bulk, 5 cm diameter×5 cm height) by using the pulsed neutron transmission spectroscopic imaging technique. Before the experiment, we developed a new CT reconstruction method, a tensor CT method. Strain tomography is quite difficult in principle. This is because the traditional CT reconstruction can deal with only “scalar” quantity although strain is “tensor”. Therefore, we developed such a new CT reconstruction method, and evaluated the validity of the method by simulation calculation studies.

We performed the pulsed neutron transmission spectroscopic imaging experiment at BL10 “NOBORU” at MLF J-PARC. The beam line conditions were w/o frame overlap chopper, w/o filters, w/o B_4C slits, and w/ rotary collimator “small”. The neutron TOF imaging detector was the GEM detector. The sample was the VAMAS neutron strain-stress analysis international standard Al cylinder. We tried to quantitatively reconstruct both the radial strain and the hoop strain of the VAMAS sample experimentally. Fig. 2 shows an example of measured Bragg-edge neutron transmission spectrum at one pixel. Aluminum Bragg edges are clearly observed. After then, we extracted d-spacing projection data, and reconstructed CT images on each strain component by the tensor CT method. Fig. 3 shows the reconstruction results. The CT image reconstruction of the hoop strain compact was

successfully carried out, but that of the radial strain one was evaluated as almost homogeneous distribution. It was found that the tensor CT method was not perfect, in particular, on the radial strain component. Therefore, we are improving the tensor CT algorithm.

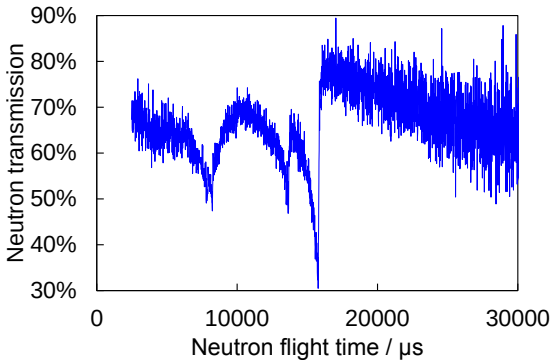

Fig. 2 Example of measured Bragg-edge neutron transmission spectrum of the VAMAS sample.

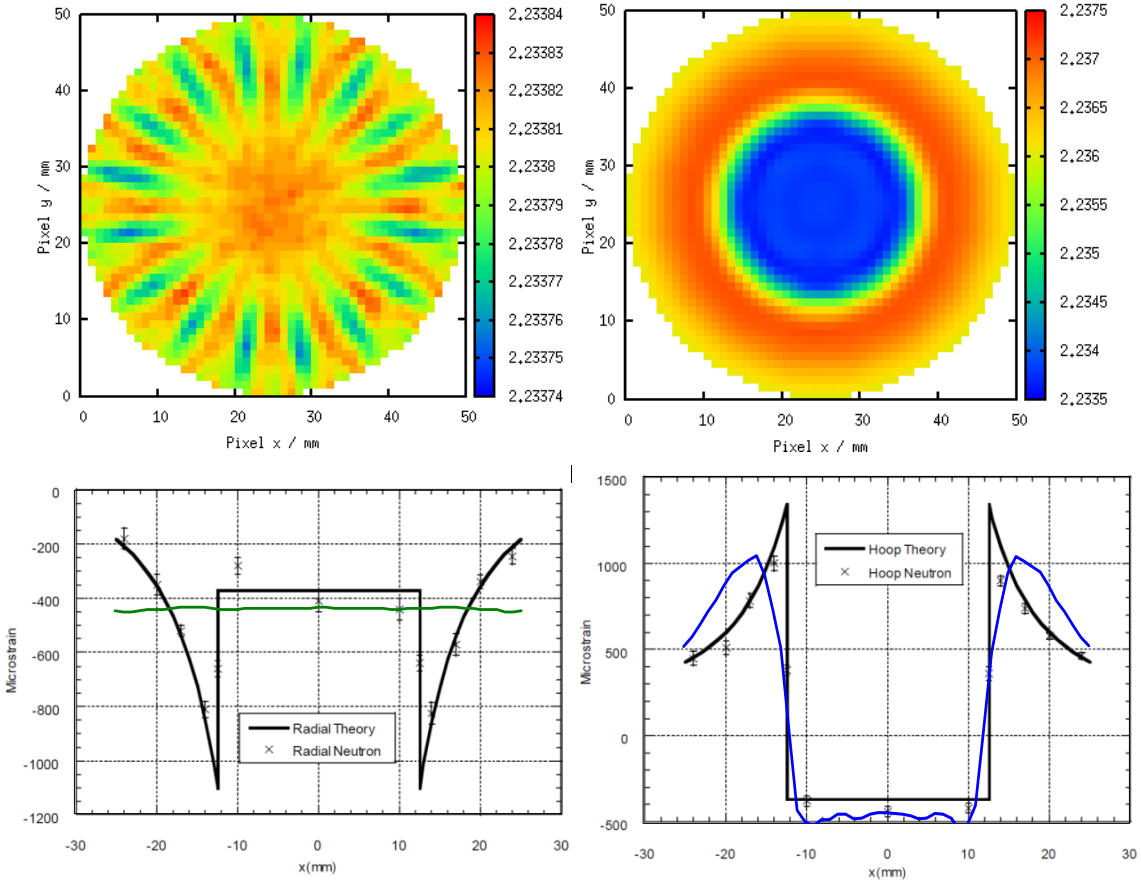

Fig. 3 Reconstructed CT images of (upper left) radial d-spacing and (upper right) hoop one, and comparison with theoretical and reconstructed values of (bottom left) radial strain and (bottom right) hoop one.

1．研究成果概要（つづき） Outline of experimental results (continued).

Ⅱ. Resonance imaging

II.1 Development of a quantitative element amount analysis

(1) Samples：

Ta, Au, Cu（for pulse function measurement）

Ta（for nuclide density quantitative evaluation）

(2) Experimental procedure and results：

The observed resonance peaks are expressed by convolution of the intrinsic resonance, the emission time distribution of neutrons emitted from a moderator and the time structure of the proton accelerator. Therefore, to perform the quantitative resonance peak analysis, the emission time distribution must be reproduced at arbitrary neutron energy by synthetic functions.

We have carried out neutron resonance absorption spectroscopy (N-RAS) experiments to measure the emission time distribution of the epithermal neutron at BL10. The emission time distribution of BL10 can be expressed by the Cole-Windsor function at arbitrary energy. We measured prompt gamma ray spectra of tantalum, gold and copper and then obtained the parameters of the function by fitting the observed resonance spectra.

Fig. 4 shows the observed resonance spectrum for the 262.4 eV resonance peak of gold. The blue line represents fitting line expressed by the convolution of intrinsic resonance, Cole-Windsor function and time structure of the proton accelerator. The effect of dual bunch structure appeared in the observed spectra and it is well fitted by synthetic function.

Fig. 5 shows the energy dependence of the parameters relating to the pulse width of the Cole-Windsor function. The broken lines represent the simulation results and the dots represent the experimental results obtained by fitting to the resonance spectra. The tendency of energy dependence of the parameters obtained in experiments almost corresponds to that of simulation. We succeeded to deduce the parameters of the emission time distribution at BL10.

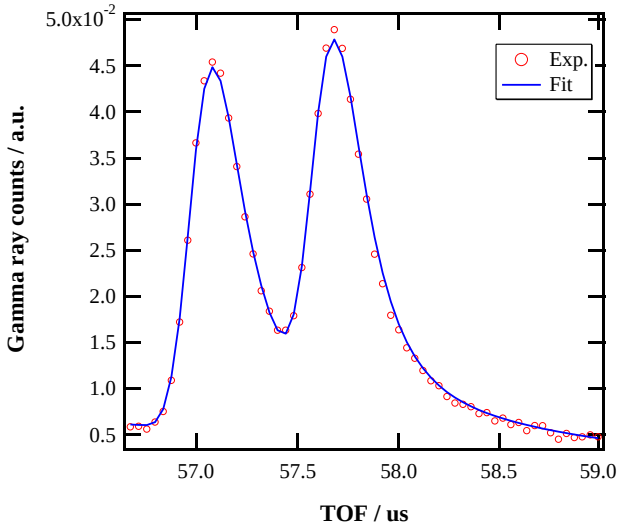

Fig. 4 The observed resonance spectrum for 262.4 eV resonance peak of gold.

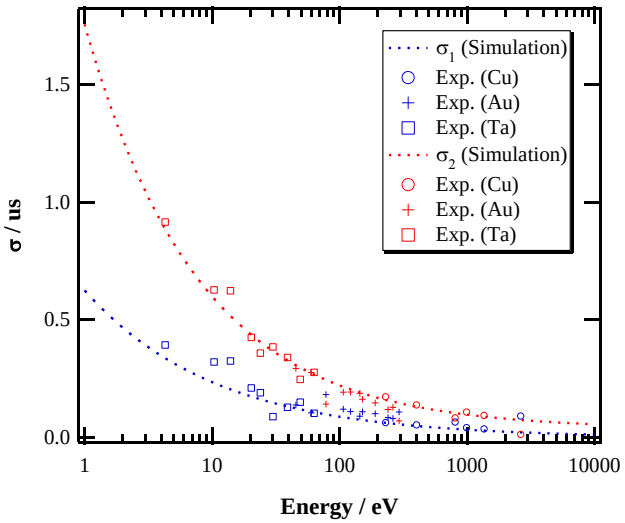

Fig. 5 The energy dependence of the parameters related pulse width of the Cole-Windsor function.

1．研究成果概要（つづき） Outline of experimental results (continued).

The neutron resonance absorption spectra contain the information of the atomic density and its motion. We can estimate the information quantitatively by analysis of the resonance peaks using the fitting code taking into account the pulse function. Therefore, we have implemented the pulse function in the resonance shape analysis code REFIT [1] to analyze the resonance peaks.

We have carried out the N-RAS experiments at BL10 to measure the transmission spectra of tantalum sample (the atomic density: 5.48×10^{-5} atoms/barn). In this experiment, we used the GEM detector, and then analyzed the observed resonance dips to estimate the atomic density of the sample using by the revised REFIT code.

Fig. 6 shows the dips caused by tantalum 4.28 eV resonance and that of 10.36 eV resonance. The blue lines represent the fitting line calculated by the code and the green dots represent the difference between the measured data and fitting. The atomic density estimated by the fitting is 5.25×10^{-5} atoms/barn within an error of ± 0.24%. It is deduced that the reason of under estimation of atomic density is caused by background arise from scattered neutron and gamma ray from the sample.

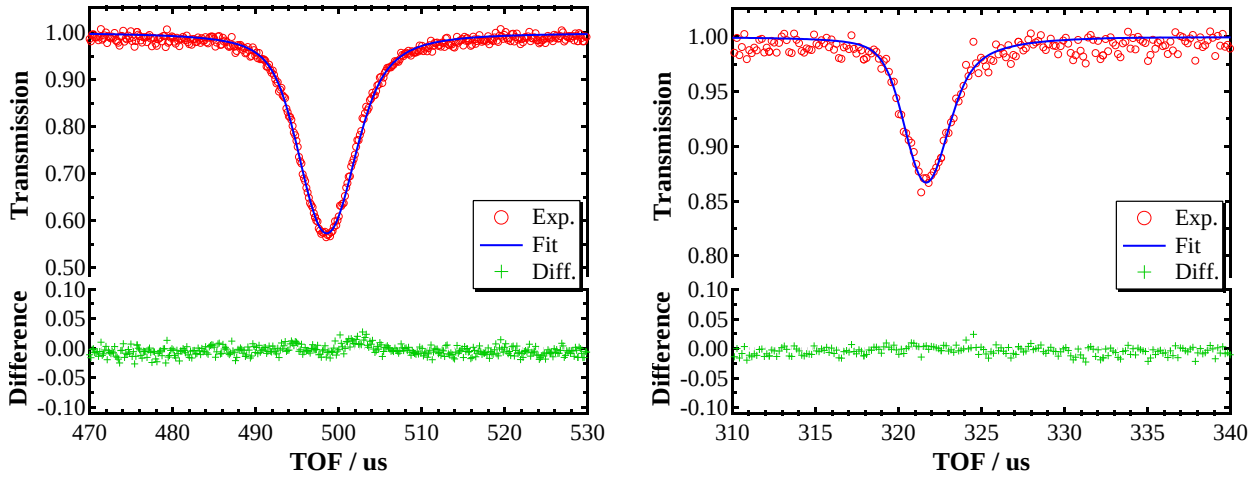

Fig. 6 The dips caused by tantalum 4.28 eV resonance (left) and 10.36 eV resonance (right).

[1] P. Schillebeeckx, et al., *Nucl. Data Sheets*, **113**, 3054-3100 (2012).

II.2 Element imaging using energy selective transmission

(1) Samples: Step-edge sample made by Fe, Cu, polyethylene and Pb in metal form.

(2) Experimental procedure and results

In this study, we aimed to construct a system for neutron energy-resolved computed tomography imaging, using a high-speed video camera system and an industrial camera system.

1. High-speed video camera system:

1-1.Experiment

Fig. 7 shows the schematic view of the experiment at BL10. The system consists of a neutron converter made of Li/ZnS (NR), lens, image intensifier (I.I.), a high-speed video camera and control-PC. An experiment was performed with use of the high-speed camera with 4k frame/sec (dT=250μsec) and the images were obtained at 45 steps of every 4 degree. The system was installed at 13.7m from neutron target.

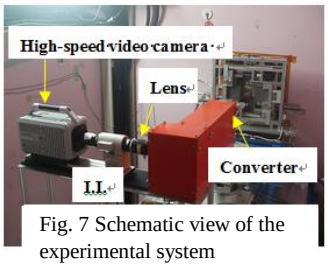

Fig. 7 Schematic view of the experimental system

Fig. 8 shows step edge samples made of Fe, Cu, Pb, and polyethylene (indicated as “poly” in this manuscript) and their size in unit of mm.

1-2. Result

Using transmission ratio images obtained by every 4 degrees step, the energy-resolved three-dimensional (3D) images were calculated by filtered back projection (FBP) method. Fig. 9 shows the calculated 3D images as volume rendering at neutron energy (En) of 4 eV and 5 meV. Comparison between the two images, the Pb was disappeared according to transmission ratio values. This result suggested that the system could visualize material alternatively by choosing neutron energy. In addition, with use of the energy dependence of each CT values, it is possible to emphasize the selected materials, even if materials such as Cu and Fe have similar energy dependence of CT values.

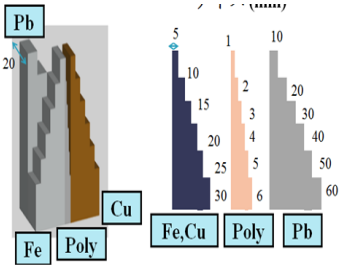

Fig. 8 Step edge sample size

The CT values on Fe and Cu derived from 3D images were shown in Fig. 10. The colored lines indicate the CT values obtained at several positions on samples. Although about 30% deviation between each data-set exists, the energy dependence of Fe and Cu CT values was marginally agreed with each other. Thus, with use of the energy dependence, we could obtain the material emphasized CT images. The left CT image of Fig. 11 emphasized Fe, subtracting from the CT values at 5 meV to that of at En= 4 meV. The right CT image emphasized polyethylene, subtracting from the CT values at En= 4 meV to that of at 4eV. The results showed that this technique has the possibility to visualize material alternatively by choosing neutron energy and emphasize materials with use of the energy dependence of CT values.

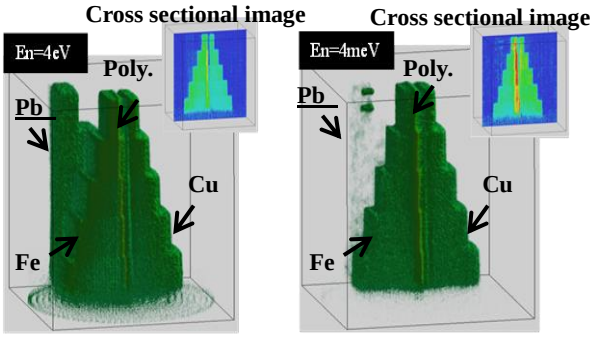

Fig. 9 Reconstructed 3D image by FBP method

Left; En=4eV(T=0.5 ms), Right;4 meV (T=15 ms)

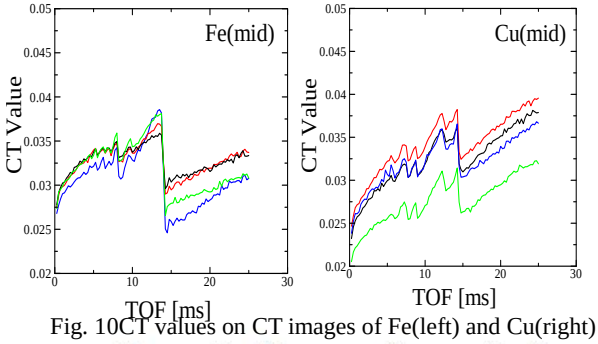

Fig. 10CT values on CT images of Fe(left) and Cu(right)

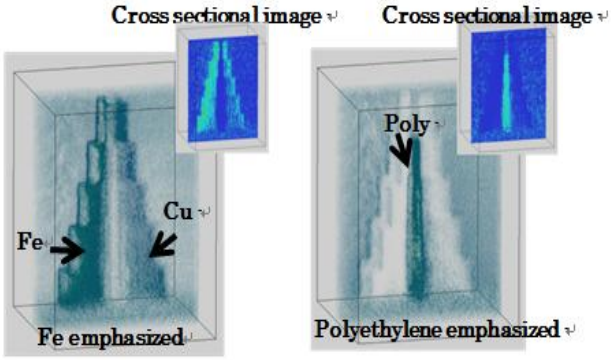

Fig. 11 Fe(Left) and polyethylene(right) emphasized 3D images

1．研究成果概要（つづき） Outline of experimental results (continued).

2. Industrial camera system

2-1. Experiment

The system consists of a NR, lens, I.I., an industrial camera and control-PC. An experiment was recorded by 25 frame/sec and the images were obtained at 36 steps of every 5 degree. Cylindrical metal foil sample made of Au, Ta and In were used as shown in Fig. 12. Neutron energy was selected at En=4.9, 4.0, 1.3 eV adjusted for Au, Ta and In resonance energy.

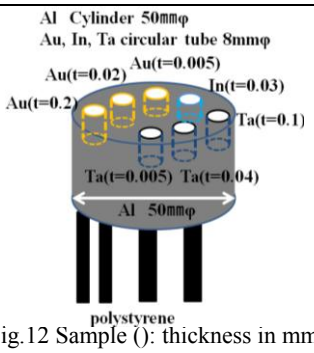

Fig.12 Sample (): thickness in mm

2-2. Result

Fig. 13 shows the CT image calculated by FBP method. They are clearly seen the cylindrical structure of the metal foil samples at resonance neutron energy. The detail is under study.

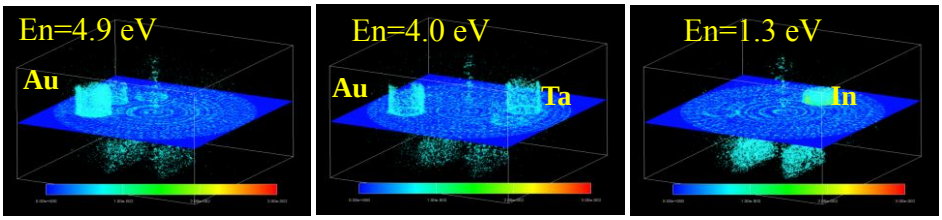

Fig. 13 Reconstructed 3D image at Au(4.9 eV), Ta(4.0 eV) and In(1.3 eV) neutron resonance energy.

III. Detector development

III.1 scintillation type detector

(1) Samples

1) ASTM sensitivity indicator, (Aluminum, Lead, Acrylic resin)

2) A spatial resolution indicator, (Gadolinium, Acrylic resin)

3) BEFs (Brightness Enhancement Films), (Acrylic resin)

(2) Experimental procedure

The pulsed-neutron imaging system consists of LiF/ZnS(Ag) scintillator and a high-speed video camera . An image intensifier was combined with the video camera, amplifying the visible light emitted from the scintillator. Samples were attached on back side of the scintillator, and transmitted neutron images were taken by the camera system.

BEFs have been used as materials for flat panel displays. Their prismatic structure focuses light toward the viewer and controls the angle of light exiting from a backlight source. Thus BEFs were attacehed on front (light-emitting) side of the scintillator and the brightness of obtained image was evaluated.

(3) Experimental results

The camera system is essentially high-resolution imaging device. The video camera has 1k x 1k pixel resolution. High-spatial-resolution imaging experiment was carried out. The sample is a newly developed line and space resolution indicator. The schematic of the indicator and the obtained image were shown in Fig. 14.

The result of spatial resolution measurement shows that the camera system has nearly 30 μm resolution that is as same as the camera pixel size.

The brightness of the fluorescence with BEFs was increased by approximately 2.5 to 3 times that of the brightness without a BEF. This technique is very promising not only for conventional neutron imaging but also for time-resolved neutron imaging.

1．研究成果概要（つづき） Outline of experimental results (continued).

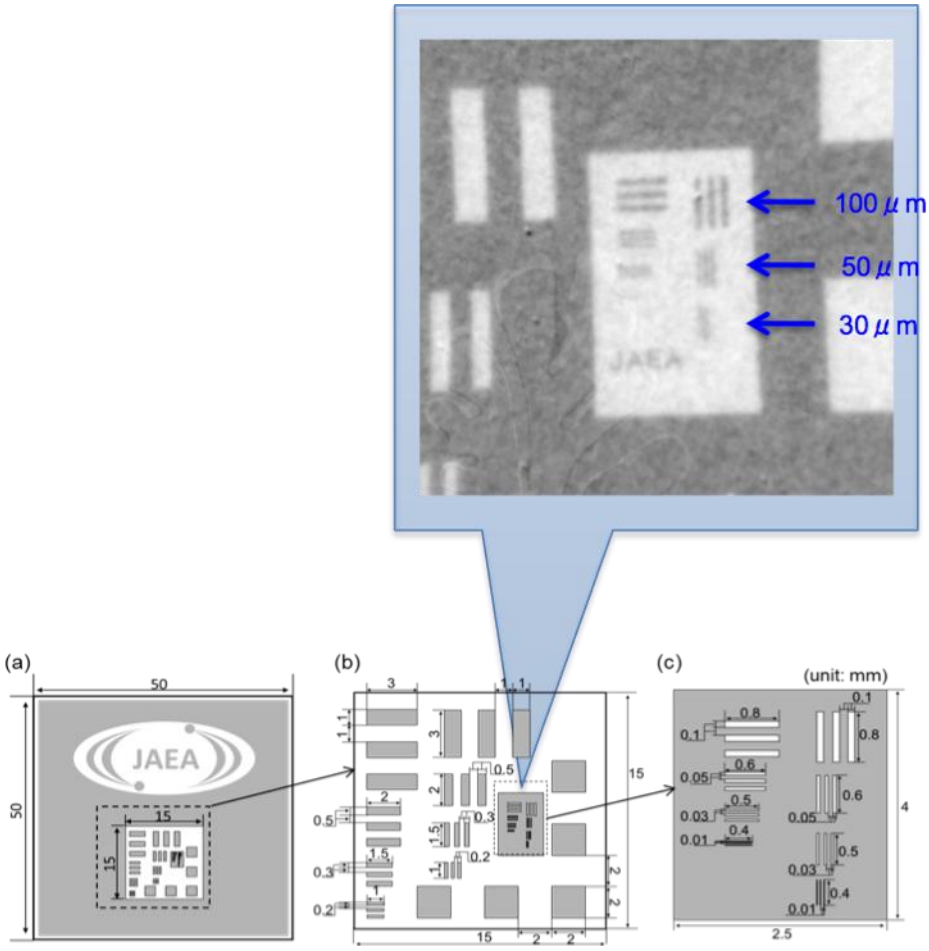

Fig. 14. Neutron image and schematic of spatial resolution indicator

III. 2 GEM type detector

(1) Sample: Fe

(2) Experimental procedure and results

We are developing a GEM type neutron detector especially for the energy-selective neutron radiography. One of key issues of this kind of detectors is how to readout two-dimensional position for one hit point. In the principle, a pulsed GEM signal can be read out using a simple double side readout strip pattern. But, we had not succeeded in this method for several years due to charge up on the front surface of the insulator. In order to avoid the charge up, the high resistive sheet was set on the front surface of the readout pattern. Then, the AC signal can penetrate the high resistive sheet and also the insulator of the readout pattern. The DC real charge can move to ground through the resistive sheet. Fig. 15 shows a correlation diagram between of the pulse heights for front and rear strips using a Fe-55 radiation source. The same amount of charge can be clearly induced for both strips. A test using the neutron beam at BL10 was performed. The 2D image could be obtained.

Two demonstrations for the energy-selective neutron radiography using GEM detector were performed. One is that the maximum event taking rate improved to 1.6MHz. It is the highest value for this kind of detectors. The second one is that a Fe absorption resonance peak (27.7keV) and corresponded two-dimensional image could be observed. It is higher energy resonance than before and even higher resonance can be seen.

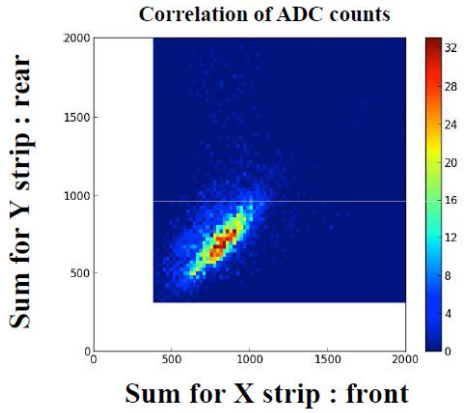

Fig. 15 A correlation diagram between the ADC counts
for front and rear strips using the simple double side readout
pattern with the high resistive sheet.

III. 3 Camera type detector

(1) Samples: Pb, Fe, Cu

(2) Experimental procedure and results

The ideal device for the technique is a time-of-flight detector with the high spatial resolution ability. One kind of the 2-dimensional position sensitive detectors has been developed as the counting type one, but it has still problems in its spatial resolution, counting rate and so on. The other candidate is photon converting type, which is assembled with the neutron to photon converting device and the photon imaging device. The detector is expected to accept the high counting rate in keeping with the high spatial resolution. The high counting rate in the intense neutron facilities is a serious problem for the transmission experiment. We are constructing the C-MOS camera type imaging device with the neutron image intensifier to avoid the difficulty of the counting rate. The detector was assembled with a high speed camera for the time sliced imaging and a vacuum tube type neutron image intensifier. There is the advantage in the neutron-photon converting that the camera can be expected higher spatial resolution than usual counters. But the huge amount of TOF image data should be transferred and recorded in the device, and we need development for the system integration. In this presentation we introduce the developed high speed camera device.

The neutron image intensifier (II) is a vacuum tube type with Gd2O5 neutron converting screen. The coming neutron was converted to the electrons in the input screen in front of the II, and then the electrons were accelerated and converged in the II. The electrons hit the II output screen and made an image. The image was reflected by a mirror behind II and taken by the high speed camera through a lens. The camera was controlled by the accelerator trigger signal, and took the time sliced image series of one neutron pulse. The images are transferred to the recording system.

The high speed camera used was the CMOS type, Mikrotron MC1362, having 1280 x 1024 pixels. The associating TOF integrated recording system was developed. The system can record the each time channel image with integrating the same time channel continuously. The recording data lengths for each time are set up as same

like 32 bit/pixel. Under the camera bright depth (8 byte), the possible recording time becomes 180 hours for 25 Hz repetition. That can be considered as enough time for the huge neutron facility. This recording system has the following advantage of the data capacity, that is, the file size is always constant.

Using the obtained TOF image series we analyzed the brightness variation spectra versus neutron flight time. Fig. 16 shows an example of TOF image series. The obtained spectra were varied correspond to the neutron spectrum, and could assign the transmitted sample specimen. Fig. 17 shows the brightness transmission spectrum and the Bragg edge feature is shown on the spectrum This result means that the developed system could be useful for the spectroscopic neutron imaging.

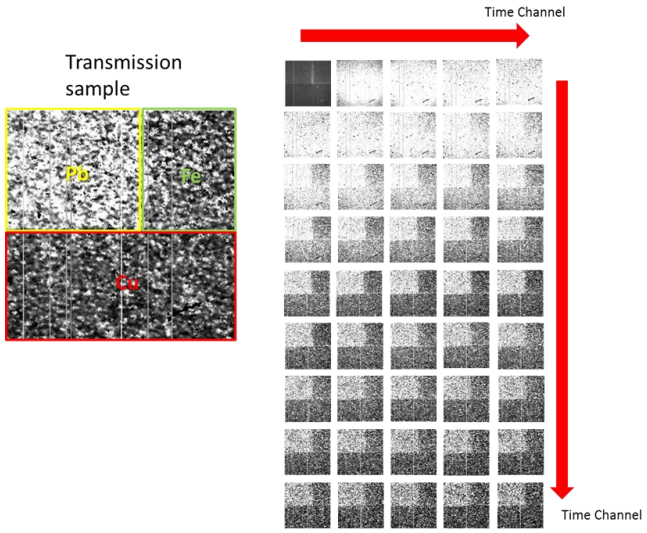

Fig. 16 TOF image series obtained by the neutron image intensifier system.
The time channel width was 0.2 ms.

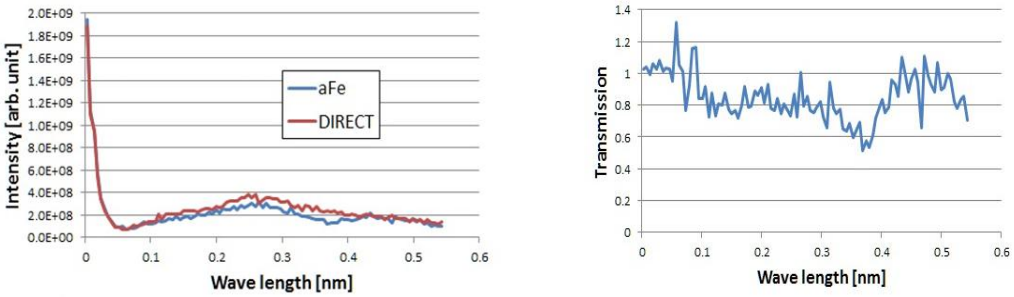

(a) Brightness spectra (b) Transmission spectrum

Fig. 17 Obtained brightness spectra from the TOF image series (a).
(b) is calculated transmission spectrum using (a)